AIP | The Journal of Chemical Physics

Structure and photoabsorption properties of cationic alkali dimers solvated in neon clusters

D. Zanuttini, J. Douady, E. Jacquet, E. Giglio, and B. Gervais

Citation: The Journal of Chemical Physics **133**, 174503 (2010); doi: 10.1063/1.3490251
View online: http://dx.doi.org/10.1063/1.3490251
View Table of Contents: http://scitation.aip.org/content/aip/journal/jcp/133/17?ver=pdfcov
Published by the AIP Publishing

Structure and photoabsorption properties of cationic alkali dimers solvated in neon clusters

D. Zanuttini, J. Douady, E. Jacquet, E. Giglio, and B. Gervais[a)]
CIMAP, Unité Mixte CEA-CNRS-ENSICAEN-UCBN 6252, BP 5133, F-14070 Caen, Cedex 05, France

(Received 16 July 2010; accepted 27 August 2010; published online 1 November 2010)

We present a theoretical investigation of the structure and optical absorption of M_2^+ alkali dimers (M=Li,Na,K) solvated in Ne_n clusters for $n=1$ to a few tens Ne atoms. For all these alkali, the lowest-energy isomers are obtained by aggregation of the first Ne atoms at the extremity of the alkali molecule. This particular geometry, common to other M_2^+-rare gas clusters, is intimately related to the shape of the electronic density of the X $^2\Sigma_g^+$ ground state of the bare M_2^+ molecules. The structure of the first solvation shell presents equilateral Ne_3 and capped pentagonal Ne_6 motifs, which are characteristic of pure rare gas clusters. The size and geometry of the complete solvation shell depend on the alkali and were obtained at $n=22$ with a D_{4h} symmetry for Li and at $n=27$ with a D_{5h} symmetry for Na. For K, our study suggests that the closure of the first solvation shell occurs well beyond $n=36$. We show that the atomic arrangement of these clusters has a profound influence on their optical absorption spectrum. In particular, the $X\Sigma$ transition from the X $^2\Sigma_g^+$ ground state to the first excited $^2\Sigma_u^+$ state is strongly blueshifted in the Frank–Condon area. © *2010 American Institute of Physics*. [doi:10.1063/1.3490251]

I. INTRODUCTION

The influence of the solvent on the dynamics of photoexcited chromophores can be investigated in great details by using charged chromophores embedded in inert gas clusters. One of the major strengths of such an approach is the possibility to select exactly the number of constituents of the cluster by simple and efficient methods of mass selection. This idea has been widely used for I_2^- molecules embedded in atomic Ar_n clusters[1–4] or in molecular clusters, such as $(CO_2)_n$ (Refs. 5–7) and $(OCS)_n$.[8] Other molecular anions, such as Br_2^- (Ref. 9) or IBr^- solvated in $(CO_2)_n$,[10] have been also studied. For all these systems, time-resolved photoelectron spectroscopy as well as mass spectroscopy of the photofragments were investigated and provide a wealth of information.

In the prototypical case of $I_2^-Ar_n$, the experimental photofragment analysis[1] combined with nonadiabatic molecular dynamics simulation[3] reveals that the dissociation of the molecule in the $A\Sigma_{g,3/2}$ state can be hindered for a number of solvent atoms as small as $n=10$, leading to geminate recombination of the I_2^- molecule. This recombination becomes more and more significant as the number of solvent atoms increases up to the closure of the solvation shell at $n=20$. Such a geminate recombination exists also for cationic systems and has been reported for $Na_2^+Ar_{17}$ clusters, i.e., for the complete first solvation shell of Na_2^+ in Ar.[11]

While both anions and cations are equivalent in terms of size selection, the anions present the distinct advantage to offer low ionization energy, which has been used to achieve time-resolved photoelectron spectroscopy experiments.[2,12] Nevertheless, alkali cations offer interesting alternatives. The excited states correlating to the first excited ^2P states of the alkali atoms present several curve crossings between Π and Σ states. These crossings turn out to conical intersections when solvent atoms are added to the system. These intersections are topologically different from the degeneracy observed at the dissociation limit of the molecules, which is responsible for the geminate recombination mentioned above. From a computational point of view, cationic alkali dimers embedded in light rare gas constitute a very appealing class of model systems. Their electronic structure is simple and they can be accurately described as one-electron systems by means of core polarization potential[13–15] so that all matrix elements for Hamiltonian forces and nonadiabatic couplings, as well as related observables, such as transition energies and oscillator strengths, are readily obtained on the same footing. It is thus possible to investigate in detail the influence of solvent atoms on the relaxation of such a photoexcited system.

In a previous paper, we establish that the confinement of Na_2^+ in a few solvating Ar atoms is able to promote the first $^2\Sigma_u^+$ state above the first $^2\Pi_u$ states in the Frank–Condon area of the ground state. This effect was however limited to sodium in a small range of cluster sizes $n=6-14$. Here, we generalize our previous work to Li_2^+, Na_2^+, and K_2^+ embedded in Ne clusters. Our ultimate goal is to investigate the nonadiabatic relaxation dynamics of photoexcited systems of well defined sizes and a preliminary study of their structure and photoexcitation properties is necessary. The choice of Ne relies in the availability of a computationally cheap and accurate parametrization of core polarization potential for these systems.[14]

Our model and the computational method have been described in detail elsewhere[11] and only their most important features are given here. The solvated alkali dimers $M_2^+Ne_n$

[a)]Author to whom correspondence should be addressed. Electronic mail: gervais@ganil.fr.

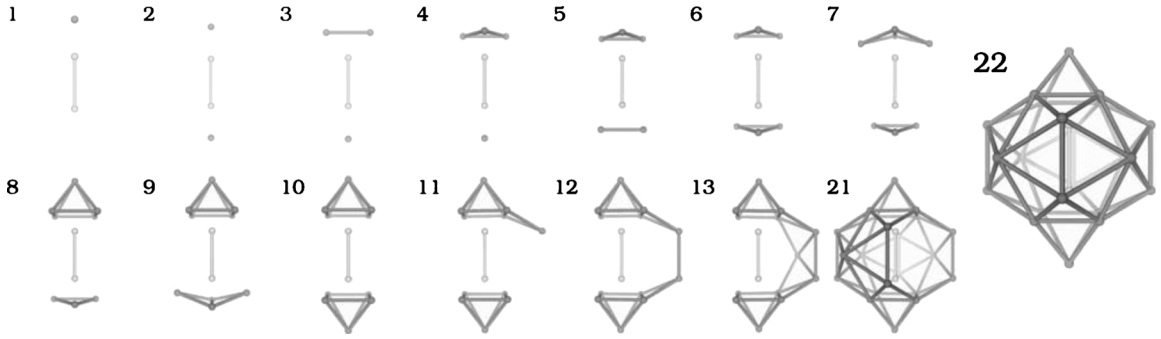

FIG. 1. Selected $Li_2^+Ne_n$ lowest-energy structures.

are described as one-electron systems, with the help of semilocal pseudopotentials complemented by core polarization potentials. The parametrization is limited here to dipole polarization terms of both M^+ and Ne cores.[14] We checked that a more accurate parametrization up to quadrupolar terms for Ne has only a marginal effect on the structure and spectral properties discussed in this paper. The Ne–Ne potential is taken from the work of Aziz and Slaman.[16] The basis set necessary to achieve an accurate computation remains rather modest, making a numerical investigation computationally easier than for Ar. The valence electronic orbitals are expanded in a basis set made of uncontracted Gaussian type orbitals centered on each alkali and Ne core. We used a large basis set made of even tempered orbitals. We used $(8s/7p/3d)$ for Li, $(12s/8p/3d)$ for Na, and $(15s/14p/5d)$ for K. We used initially a $(2s/2p/1d)$ basis set for Ne, which was further reduced to $(1s/1p)$ basis optimized to reproduce the ground and excited states of the MNe dimers correlating asymptotically with the lowest ^2S and ^2P states of the alkali M. Reducing the basis set centered on Ne atoms has a rather small effect on the transition energies. For $Li_2^+Ne_{22}$ as an example, the $X\Sigma$ and $X\Pi$ transition energies are reduced by 20 and 17 meV, respectively, i.e., by less than 1%.

The main strength of our approach is to provide all observables concerning the $M_2^+Ne_n$ clusters in the same footing. In particular, the structures discussed in Sec. II and the related spectroscopic properties presented in Sec. III are obtained at the same level of description. Note that only static structures were determined in this work. The dynamics of the aggregation process, which does not necessarily lead to the formation of the lowest-energy isomer, is beyond the scope of the present work. Atomic units $(\hbar=e=m_e=1)$ are used throughout the paper, unless otherwise stated.

II. STRUCTURES

The geometry of each system is obtained from an initial guess of its structure, based on consideration of the relative bonding strength of M_2^+–Ne and Ne–Ne and from our previous experience on $Na_2^+Ar_n$ systems. For each cluster size n, several initial arrangements were relaxed by means of dissipative molecular dynamics. The relaxation consists in resetting the velocity $\mathbf{v}_a$ of the atom a to $\mathbf{v}_a=\mathbf{0}$ when the scalar product between $\mathbf{v}_a$ and the force $\mathbf{F}_a$ experienced by the atom $\mathbf{v}_a\cdot\mathbf{F}_a$ becomes negative. Each structure was annealed to 30 K after relaxation to check its stability. Approximately 600 stable structures were obtained in this way for all types of cations.

The structures of a selected set of the lowest-energy isomers we found are presented in Figs. 1–3 for $Li_2^+Ne_n$, $Na_2^+Ne_n$, and $K_2^+Ne_n$, respectively. From these figures, general trends common to all three systems emerge clearly. First of all, nucleation proceeds by adding Ne atoms at the extremities of the alkali dimer. This feature was observed for $Na_2^+Ar_n$ and is common to all M_2^+ rare gas clusters. It can easily be understood by considering the shape of the ground state electronic density of the M_2^+ molecules, which are depicted in Fig. 4. The neon atoms tend to minimize their overlaps with the electronic cloud located between the two alkali ions, where the Pauli repulsion between the alkali valence electron and the neon electrons dominates. On the contrary, the polarization energy of the systems is lowered by optimizing the M^+–Ne bond. Such a balance between Pauli repulsion and polarization attraction is quite general for ionic molecules embedded in a rare gas solvent and it is observed for anionic halogen dimers as well. In the latter case, however, the electronic density of the $^2\Sigma_u^+$ ground state of homonuclear

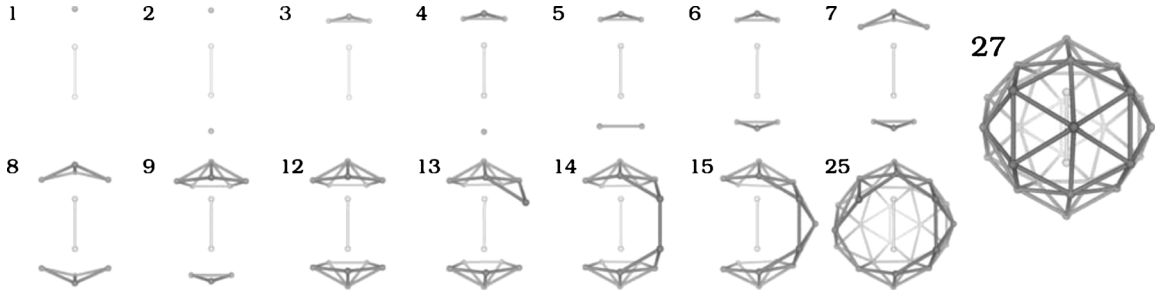

FIG. 2. Selected $Na_2^+Ne_n$ lowest-energy structures.

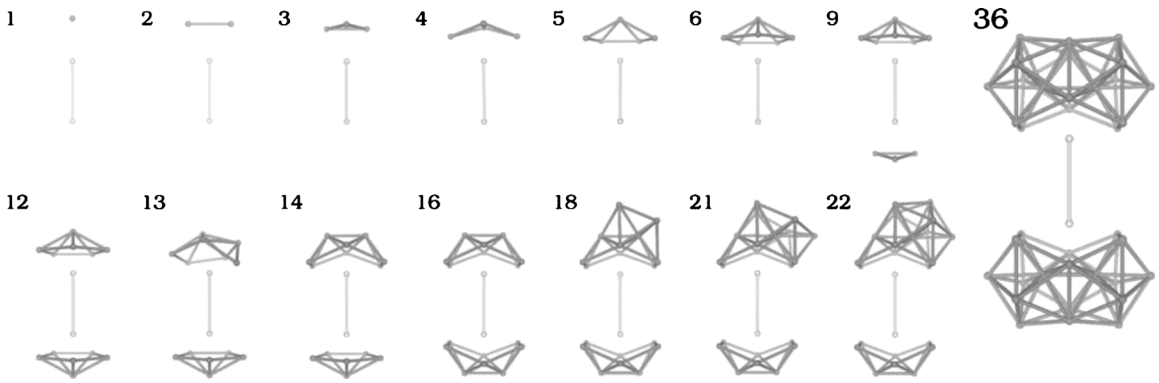

FIG. 3. Selected $K_2^+Ne_n$ lowest-energy structures.

dimers is larger at the extremities of the molecule, as depicted in Fig. 4 for some halogen anions, so that the nucleation starts in the symmetry plane perpendicular to the molecular axis.[3,4]

The second common feature to all these clusters is the development of triangular Ne_3 motifs and of pentagonal Ne_6 pyramids, which are characteristic of icosahedral ordering observed in pure rare gas clusters.[17,18] These structural motifs favor large coordination number for each Ne atom in the system. It is interesting to note that for a given cluster size n, most of the equilibrium geometries found for a given alkali correspond also to equilibrium geometries for the other alkali. This feature is however modulated when changing the nature of the alkali so that for a given number n of Ne atoms, the geometry of the most stable isomer may change from one alkali to another one. The difference can be rationalized by considering the binding properties of a single Ne atom to each akali dimer, which are summarized in Table I. The ratio of the M_2^+–Ne binding energies to the Ne_2 molecule binding energy is 24:11:6 for M=Li, Na, and K, respectively.

For $n \leq 6$, $Li_2^+Ne_n$ and $Na_2^+Ne_n$ have the same geometries, at the exception of $n=3$. In this case the strong Li_2^+–Ne bond favors bonding at both extremities of the Li_2^+ molecule, at the expense of the coordination number of the Ne atoms. This is the only case for which the Ne_3 triangular motif is not favored in the whole series of lowest-energy isomers we investigated. In this range of size, the $K_2^+Ne_n$ equilibrium geometries are obtained by increasing the number of Ne atoms at one single extremity. This peculiarity reflects the longer K_2^+–Ne bond, which allows fitting more equivalent Ne atom in the same potential well.

For $7 \leq n$, both extremities are progressively filled, until a highly symmetric arrangement is obtained at $n=10$ for Li and $n=12$ for Na and K. Here again the strong Li_2^+–Ne bond favors a tight D_{4h} symmetry, while the shallower bond favors a D_{5h} symmetry for both Na and K. However, it is interesting to note that both MNe_p structures at the extremities of the molecules corresponds to the minimum energy structures of rare gas clusters made of $(p+1)$ atoms, in particular, Ar_{p+1}.[17]

Beyond this limit, the structures develop until completion of the first solvation shell with D_{4h} symmetry at $n=22$ for Li and with D_{5h} symmetry at $n=27$ for Na. In the case of K, we do not obtain a closed solvation shell for $n \leq 36$. In this case indeed, the most stable isomers are obtained by increasing the coordination number of Ne atoms and by starting building additional shells of Ne atoms. The origin of this difference can be traced back by a closer comparison of $K_2^+Ne_n$ and $Na_2^+Ne_n$ for $n=12-14$. We identify two mechanisms responsible for this difference: the rocking of the Ne motif and an increased alkali bond length for K_2^+. For $Na_2^+Ne_{13}$, the addition of one Ne atom to the highly symmetric $Na_2^+Ne_{12}$ does not perturb much the original structure. On the contrary, for $K_2^+Ne_{13}$, the additional Ne atom induces a significant rocking of the upper Ne_6 cap to which it is bounded. This rocking is possible for the shallow K_2^+–Ne bond, while a similar rocking for the Na system induces more overlap between the Na valence electronic cloud and

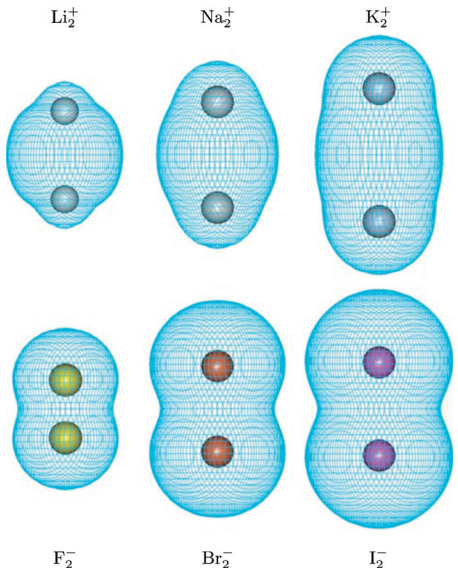

FIG. 4. Electronic density contour plot for alkali cationic dimers (Li_2^+, Na_2^+, K_2^+) and halogen anionic dimers (F_2^-, Br_2^-, I_2^-). The contour is taken to include 99.9% of the whole electronic density.

TABLE I. Binding energy, D_e, and equilibrium distance, R_e, of the M_2^+–Ne systems in C_∞ symmetry; R_e is the distance between the Ne atom and the closest alkali. The binding energy and equilibrium distance of the Ne_2 molecule are given for comparison.

	Li_2^+–Ne	Na_2^+–Ne	K_2^+–Ne	Ne–Ne
R_e (a.u.)	3.97	4.89	5.78	5.80
D_e (meV)	87.3	40.0	21.8	3.6

the Ne core electrons. The second important difference between Na and K comes from the bond length difference between K_2^+ ($R_e \approx 8.5$ a.u.) and Na_2^+ ($R_e \approx 6.8$ a.u.). For $n=14$, it is thus possible to bridge the upper and lower Ne_7 motifs of $Na_2^+Ne_{14}$ by a Ne–Ne bond, whose length is only slightly perturbed with respect to the free Ne_2 molecular bond. On the contrary, for the $K_2^+Ne_{14}$ isomer with the same geometrical arrangement as $Na_2^+Ne_{14}$, the Ne–Ne bonding distance between the upper and lower Ne_7 motifs is much longer. It is thus more favorable to build an asymmetric structure made of 8 Ne atoms at one extremity and 6 at the other one, as depicted in Fig. 3, although the coordination number is the same for both isomers. The combined effect of rocking and Ne–Ne bond stretching results in an energy difference of 7 meV between the lowest-energy isomer of $K_2^+Ne_{14}$ and its counterpart with the same structure as the lowest-energy isomer of $Na_2^+Ne_{14}$.

It is interesting to note that the KNe_8 structure observed on top of the $K_2^+Ne_{14}$ cluster in Fig. 3 presents the same geometry as the lowest-energy isomer obtained for Ar_9.[17] Starting from these structures at both extremities of the K_2^+ molecule for $n=16$, the $K_2^+Ne_n$ clusters develop by increasing the coordination number of the Ne atoms with a close packing icosahedral arrangement, without bridging the Ne structure at the opposite extremities of the K_2^+ molecule. Adding up to 36 Ne atoms results in a symmetric cluster, made of two identical KNe_{18} structures, which geometry is the same as the geometry of the lowest-energy isomer found for Ar_{19}.[17] Above this limit, we expect the $K_2^+Ne_n$ clusters to develop like bare rare gas clusters until the substructure at both extremities merge to form a complete solvation shell around K_2^+.

For all three systems, we have plotted in Fig. 5 the binding energy difference defined as

$$\Delta E_n = E_{n-1}^* - E_n, \tag{1}$$

where E_n is the binding energy of a given isomer of $M_2^+Ne_n$ cluster and E_n^* is the binding energy of the corresponding lowest-energy isomer. All the curves converge progressively toward a value comparable to the cohesion energy of bulk Ne, E_{coh}, which we calculated to be $E_{coh} \approx 27$ meV. Note that this value of the cohesion energy neglects the zero-point energy motion, as our potential energy values do. For $Li_2^+Ne_n$ clusters, the large binding energy difference with respect to E_{coh} for $n \leq 6$ indicates an enhanced stability of these clusters, which are probably easier to observe experimentally. The large difference observed between ΔE_n and ΔE_{n+1} at $n=2,6$ and to a lesser extent at $n=10$ reveals the enhanced stability of these clusters. For Na and K, we do not observe a domain in which ΔE_n is significantly larger than E_{coh}. However, we observe enhanced ΔE_n correlated with reduced ΔE_{n+1} at $n=3,6,12$ for Na and K, which reveals the enhanced stability of these clusters (Fig. 5). It is interesting to note that for these sizes, the binding energy difference $E_n - E_n^*$ between the second lowest-energy isomer and the lowest-energy isomer that we found is significantly larger than for the other values of n. For K, the variation of ΔE_n for $n=7-12$ is very similar to its variation of $n=1-6$, which reflects nicely the aggregation at one extremity for $n=1-6$ and then at the other one with the same arrangements for $n=7-12$. For n ranging from 14 to 31, all the lowest-energy structures were obtained with the same Ne_8 motif at one extremity and $(n-8)$ Ne atom at the other one. We observe maxima of ΔE_n at $n=14,16,22,26,30$, which reflects an enhanced stability of the corresponding $Ne_{p=n-8}$ structures. Among the corresponding KNe_p structures, those for $p=6,8,18$ have the same geometries as the pure Ar_{p+1} lowest-energy isomers.[17] The latter structure seems particularly stable so that for n ranging from 32 to 36, all the lowest-energy structures were obtained with the same Ne_{18} motif at one extremity and $(n-18)$ Ne atom at the other one.

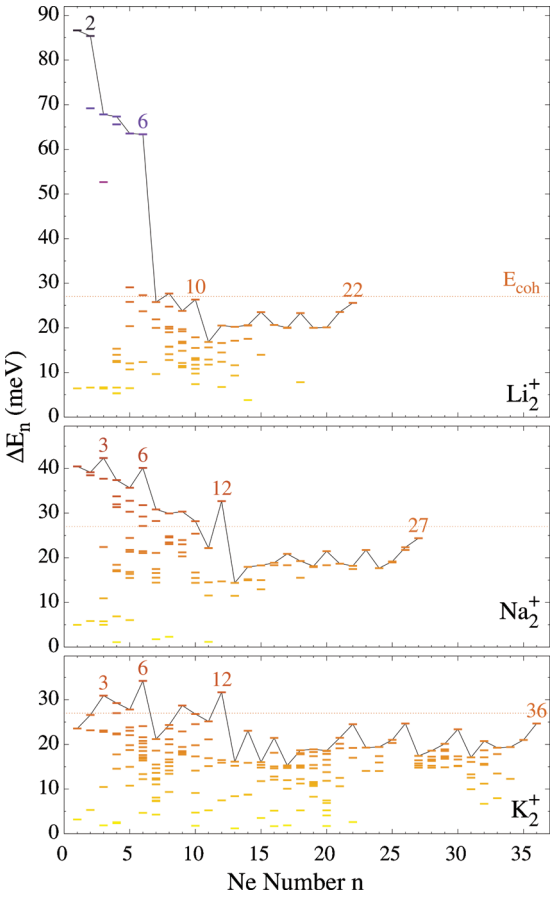

FIG. 5. Binding energy difference ΔE_n. Each dash corresponds to a stable isomer we found. The line joins the most stable isomers.

III. ABSORPTION SPECTRUM

The optical absorption of the system can be calculated in the Frank–Condon approximation from its electronic structure and the Condon factor. The latter is not easy to obtain when continuum states are coupled to bound states by nonadiabatic couplings. Moreover, the inclusion of all rovibrational levels becomes rapidly cumbersome as the size of the system increases. Following the idea of Lax[19] and Heller,[20] we computed the oscillator strength of the transitions from the electronic ground state 0 to an excited state a for a transition energy ω as

$$\frac{\partial f}{\partial \omega} = \bar{f}_{0a}(\omega)$$

$$= \frac{2}{3}\int d\mathbf{R}\omega_{a0}(\mathbf{R})|\langle 0|\mathbf{r}|a\rangle|^2\rho_0(\mathbf{R})\delta(\omega-\omega_{a0}(\mathbf{R})), \quad (2)$$

where $\rho_0(\mathbf{R})$ is the ground state probability density to find the system at a geometry characterized by the complete set of atomic positions of the system $\mathbf{R}$ and $\omega_{a0}(\mathbf{R})=E_a(\mathbf{R})-E_0(\mathbf{R})$ is the difference of the electronic energies of states a and 0 at position $\mathbf{R}$. For light atoms, such as Li and Ne, it is necessary to take into account the zero-point vibrational motion. We have therefore computed the quantum probability density $\rho_0(\mathbf{R})$ for the ground state in the harmonic approximation. The transition energies $\omega_{a0}(\mathbf{R})$ were not corrected for the vibrational energies. We first determined the Hessian matrix elements H_{ij} for the electronic ground state by using a finite difference scheme,

$$H_{ij} = \frac{1}{\sqrt{m_i m_j}}\frac{\partial^2 E_0}{\partial R_i \partial R_j} = \frac{F_i(\mathbf{R}^0+\delta\mathbf{u}_j)-F_i(\mathbf{R}^0-\delta\mathbf{u}_j)}{2\sqrt{m_i m_j}\delta}, \quad (3)$$

where $\mathbf{R}^0$ is the equilibrium position of the system, $\mathbf{u}_j$ is the unit vector in the direction of the jth component of $\mathbf{R}$, m_i is the corresponding mass, and δ is the amplitude of the displacement along $\mathbf{u}_j$ to perform the finite difference. In the harmonic approximation, the distribution of modes $\rho_0(\mathbf{q})$ is simply a product of Gaussian functions $g_\nu(q_\nu)$, which can easily be sampled to perform the $3n$-dimensional integral of Eq. (2) by a Monte Carlo sampling of the vibrational modes q_ν. For a sampled vector $\mathbf{q}$, the positions of the atoms are obtained as $\mathbf{R}=\mathbf{R}^0+Q^T\cdot\mathbf{q}$, where Q is the matrix of normalized eigenmodes expressed as a function of Cartesian displacement coordinates. For nonbridged isomers, a soft mode is associated to the rotation of the two capping blocks of Ne atoms around the M_2^+ axis. The harmonic approximation is no longer valid in this case. However, this mode is well decoupled from the other ones and we can mimic the effect of the corresponding slow rotation by sampling uniformly the rotation angle instead of the mode itself.

Since the transitions occur in an area of potential energy surface crossing, the assignment of the transitions from adiabatic excited states is not very telling. Around such a crossing, the adiabatic states change of character from mainly Σ to mainly Π symmetry in the case of alkali dimers. An example of this crossing is presented in Fig. 6 in the case of the bare Li_2^+ molecule. For a better identification of the transition we labeled Σ the state corresponding to a transition dipole $\langle 0|\mathbf{r}|a\rangle$ that maximizes the component oriented along the M_2^+ molecular axis. The two other states are labeled Π and sorted according to their energies.

The possible effect of a small amount of internal excitation energy has been investigated by changing the distribution $\rho_0(\mathbf{R})$ by the corresponding distribution for a harmonic bath in equilibrium at a finite temperature $T=15$ K. We do not observe significant changes and we shall limit our discussion to the ground vibrational state of the system.

A selected set of absorption spectrum is presented in Fig. 7 for the three alkali and several values of n. The bare M_2^+ spectrum is dominated by two intense absorption peaks corresponding to the $X\Sigma$ transition from $X\ ^2\Sigma_g^+$ to $A\ ^2\Sigma_u^+$ state and to the two $X\Pi$ transitions from the $X\ ^2\Sigma_g^+$ to the degenerated $B\ ^2\Pi_u$ states. In the bare molecule, the first $^2\Sigma_u^+$ state is strongly repulsive in the Frank–Condon area and leads to the dissociation of the molecule for the three alkali. On the contrary, the first $^2\Pi_u$ states are bonding and a discrete set of transitions associated to the rovibrational states could be observed. We do not attempt to resolve the corresponding structures and concentrate here on the effect of the surrounding Ne atoms on the absorption spectrum.

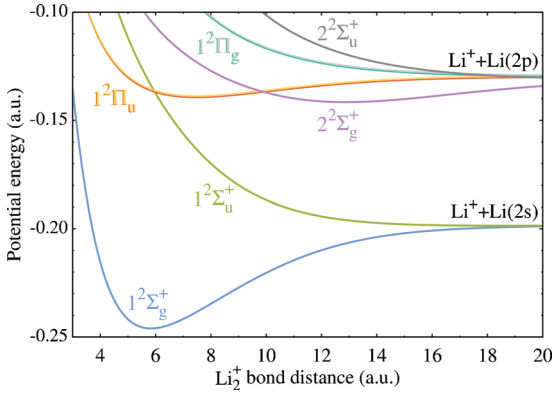

FIG. 6. Potential energy curves of the lowest-energy states of the bare Li_2^+ molecule.

The steepness of the potential energy surface (PES) associated with the first $^2\Sigma_u^+$ state leads to a broad absorption peak whatever the size and isomer of the cluster. On the contrary the peaks associated to the first $^2\Pi_u$ states are narrower and a more or less pronounced separation of the two $X\Pi$ absorption peaks can be observed, according to the symmetry of the isomer.

The increase of Ne atoms in the cluster leads to a huge spectral shift of the $X\Sigma$ transition. This feature is common to all three alkali systems and could certainly be observed experimentally. It is similar to the spectral shift observed previously for $Na_2^+Ar_n$ clusters. The origin of this shift arises from the confinement of the σ_u orbital of the alkali molecule. This is illustrated in Fig. 8, where we compare the orbitals of the bare Li_2^+ molecule to those of $Li_2^+Ne_{22}$. We see clearly that the σ_u orbital deforms to minimize the overlap with the Ne cores. The π_u orbitals are less sensitive to the presence of the surrounding Ne atoms. The main reason is that the σ_u orbital is more directional and concentrated around the tip of the molecule where the Ne atoms are located at relatively short distance from the alkali centers, while the π_u orbital expands around the equatorial plane where these distances are larger. This effect is observed for all structures obtained by relaxation on the $X\ ^2\Sigma_g^+$ PES and it is stronger for the structures with moderate n, for which the equatorial plane is free of any Ne atom. The relaxation on another PES with different symmetries could of course lead to a different result.

The respective positions of the $X\Sigma$ and $X\Pi$ transitions depend on the nature of the alkali dimer. For bare Li_2^+, the crossing between the first $^2\Sigma_u^+$ and $^2\Pi_u$ states is located in the Frank–Condon area. When adding Ne atoms, the $X\Sigma$ transition is strongly blueshifted, and the corresponding transition takes place at a higher energy than the $X\Pi$ transitions. An

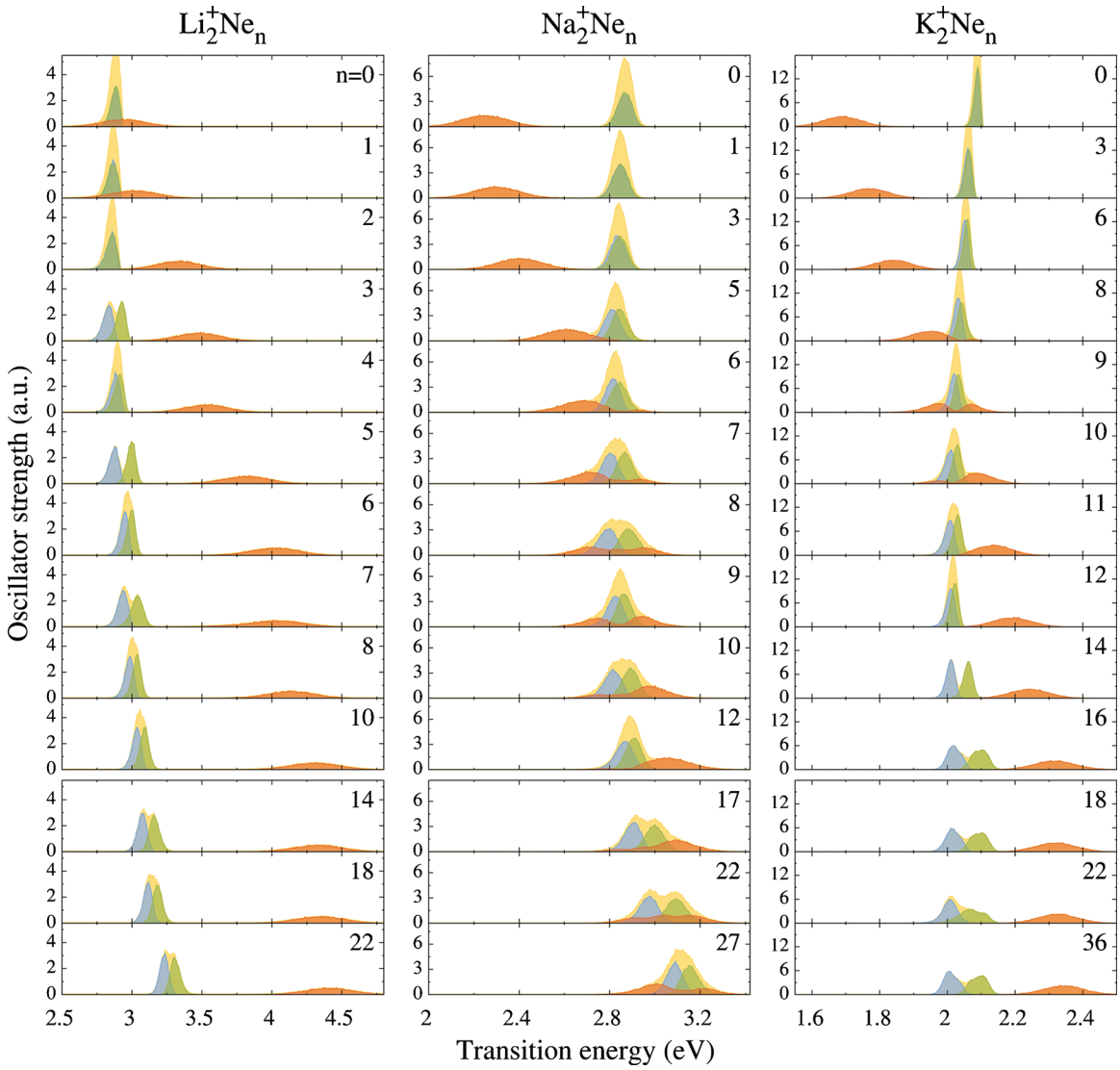

FIG. 7. Oscillator strength spectrum of the lowest-energy isomers for some selected cluster sizes n. Orange peak: XΣ transition; blue and green peaks: XΠ transition; yellow peak: sum of the transitions.

overlap between the two absorption peaks exists only for $n=1$, for which the coupling between $^2\Sigma_u^+$ and $^2\Pi_u$ states induced by the vibrating Ne atom is relatively weak. The large separation between the absorption peaks for larger sizes offers an interesting situation for photoexcitation experiments. Indeed, when excited in the dissociative $^2\Sigma_u^+$ state, the Li_2^+ molecule stretches to minimize its potential energy so that the system will necessarily reach the conical intersection at the crossing between $^2\Sigma_u^+$ and $^2\Pi_u$ states, offering thus several rearrangement pathways.

For bare K_2^+, the crossing between the first $^2\Sigma_u^+$ and $^2\Pi_u$ states is not located in the Frank–Condon area and three different situations are observed when the number of Ne atoms increases. For $n \leq 8$ the ordering of the first $^2\Sigma_u^+$ and $^2\Pi_u$ states is not changed with respect to the bare K_2^+ molecule and a more or less adiabatic dynamics may be expected after photoexcitation in one of these states. For $11 \leq n$, we observe the opposite situation, somewhat comparable to the case of $Li_2^+Ne_n$ clusters. Beyond $n=16$, the relative flatness of the PES in the Frank–Condon area splits the $^2\Pi_u$ absorption band in two peaks. The shape of the absorption band is governed by the soft mode associated to the rotation of the upper and lower Ne blocks at the extremity of the M_2^+ molecule. For geometries close to D_{2d} symmetry, this band reduces to one single peak, but these geometries have a small statistical weight.

For $n=9$, and to a some extent for $n=10$, the situation is different. The peak associated to the XΣ transition splits in two peaks located on both sides of the narrow XΠ absorption. This peculiar feature is related to the C_3 symmetry of the cluster, which does not lift the Π_u degeneracy of the cluster so that the XΠ absorption peak remains narrow. The perturbation induced by the vibrational deformation of the molecule is much more efficient to lift the degeneracy between the $^2\Sigma_u^+$ and $^2\Pi_u$ states at the conical intersection because of the steepness of the $^2\Sigma_u^+$ PES. According to the deformation of the molecule, the $^2\Sigma_u^+$ state is pushed either below or above the Π_u states. As a result, the total absorption spectrum made of the sum of all absorption peaks is dominated in its middle by absorption in the Π_u states and on both wings by absorption in the $^2\Sigma_u^+$ state.

For $Na_2^+Ne_n$, the evolution of the absorption spectrum

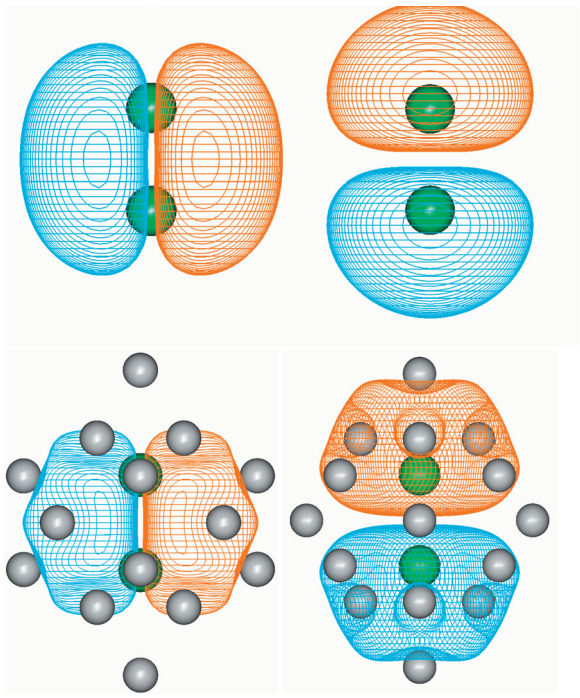

FIG. 8. Orbital contour plot for bare Li_2^+ molecule (top) and $Li_2^+Ne_{22}$ cluster (bottom). The contours are taken to include 99% of the valence electronic density. Left hand side: π_u orbital; right hand side: σ_u orbital.

with the number of Ne atoms n is quite similar to the evolution of the $K_2^+Ne_n$ spectra for $n \leq 12$. For the lowest n, the $X\Sigma$ transition appears at a lower energy than the $X\Pi$ transition. For $n=7-10$ a pronounced overlap of both transitions occurs. For $n=9$ the $X\Sigma$ band splits in two bands, which forms the wings of the total absorption spectrum, exactly like for the $K_2^+Ne_9$, which possesses the same geometry. For $n=8$ the spectrum is more complex. In this case, the D_{2d} and D_{2h} isomers are degenerate and the vibrational spectrum presents a soft mode associated to the rotation of the Ne_4 substructures around the molecular axis. The averaged spectrum resulting from uniform rotational angle sampling is presented in Fig. 7. We see that the coupling between the Σ_u^+ and Π_u states due to the vibrational motion induces a redistribution of the spectral density associated to the $X\Sigma$ transition, which is distributed over a wide range of energy in this case. Above $n=12$, the progressive closure of the first solvation shell as n increases induces also a confinement of the valence π_u orbitals. The corresponding $X\Pi$ transition becomes thus slightly blueshifted and is not well separated from the $X\Sigma$ transition, as it is the case for $Li_2^+Ne_n$ and $K_2^+Ne_n$. A similar effect was observed for $Na_2^+Ar_n$ clusters.[15]

IV. CONCLUSION

Our theoretical approach based on core polarization pseudopotential provides a powerful tool to investigate cationic alkali dimers (M_2^+) solvation in Ne clusters. We emphasized that a major strength of such an approach is to provide the structure, vibrational modes, and oscillator strength in the same unique approach, which guarantees the consistency of the results. For all alkali, the growth sequence starts systematically at the extremities of the M_2^+ molecule. This result is similar to the case of $Na_2^+Ar_n$ clusters and opposite to the nucleation reported for I_2^-, which starts in the symmetry plane perpendicular to the molecular axis. The difference between these two classes of systems can be rationalized by comparing the contour of the electronic density of these systems. Indeed, all the alkali molecules M_2^+ present a slight excess of density between the two M centers, while the halogen dimers X_2^- present a small depletion. The closed shell rare gas atoms have a propensity to localize where the density is the lowest to minimize the Pauli repulsion so that polar location is preferable for alkali, while equatorial positions are preferable for halides.

Our study shows clearly that the structure of these clusters depends on the nature of the alkali, and more specifically on the size of the cation. The tight Li_2^+–Ne bound favors compact structures, while the nucleation is rapidly dominated by the Ne–Ne interaction for the looser K_2^+–Ne bound. We observe more tightly bound clusters at $n=2,6,10$ for Li and at $n=3,6,12$ for Na and K. The corresponding Ne motifs are typical from icosahedral structures observed in small rare gas clusters and form the basis of the $M_2^+Ne_n$ clusters geometry. The closure of the first solvation shell is observed at $n=22$ with D_{4h} symmetry for Li and at $n=27$ with D_{5h} symmetry for Na. For the larger K_2^+ molecule, the closure of the first solvation shell occurs for n much larger than 36, which is the biggest cluster investigated here.

The optical absorption properties are intimately linked to the structure of the clusters. The capping at the extremities of the alkali dimers has a profound influence on the position of the first excited $^2\Sigma_u^+$ state, and the $X\Sigma$ transition is strongly blueshifted as the number of Ne atoms increases. The shift is particularly large for the compact $Li_2^+Ne_n$ clusters, where it amounts to 1.5 eV for the complete solvation shell at $n=22$. The first excited $^2\Pi_u$ states are much less affected by the presence of the surrounding Ne atoms. When the number of Ne atom becomes sufficiently large, the $^2\Sigma_u^+$ state confinement is strong enough to push this state above the $^2\Pi_u$ states in the Frank–Condon area. A similar effect has been observed for $Na_2^+Ar_n$ clusters as well, and due to its nature is likely to be observed for any rare gas and alkali. Such a large confinement effect could certainly be observed experimentally by photoabsorption techniques.

Finally, cationic alkali dimers embedded in light rare gas clusters provide a whole class of simple model systems, which allows investigating the relaxation dynamics of a photoexcited molecule solvated in a selected number of solvent atoms for various topologies of the potential energy surface.

[1] V. Vorsa, P. J. Campagnola, S. Nandi, M. Larsson, and W. C. Lineberger, J. Chem. Phys. **105**, 2298 (1996).
[2] B. Jefferys Greenblatt, M. T. Zanni, and D. M. Neumark, J. Chem. Phys. **111**, 10566 (1999).
[3] V. S. Batista, and D. F. Cocker, J. Chem. Phys. **106**, 7102 (1997); **110**, 6583 (1999).
[4] J. Faeder, N. Delaney, R. E. Maslen, and R. Parson, Chem. Phys. Lett. **270**, 196 (1997).
[5] J. M. Papanikolas, J. R. Gord, N. E. Levinger, D. Ray, V. Vorsa, and W. C. Lineberger, J. Phys. Chem. **95**, 8028 (1991).
[6] C. J. Margulis and D. F. Coker, J. Phys. Chem. **110**, 5677 (1999).
[7] B. Jefferys Greenblatt, M. T. Zanni, and D. M. Neumark, J. Chem. Phys. **112**, 601 (2000).
[8] A. Sanov, S. Nandi, and W. C. Lineberger, J. Chem. Phys. **108**, 5155

(1998).
[9] M. L. Alexander, N. E. Levinger, M. A. Johnson, D. Ray, and W. C. Lineberger, J. Chem. Phys. **88**, 6200 (1988).
[10] V. Dribinski, J. Barbera, J. P. Martin, A. Svendsen, M. A. Thompson, R. Parson, and W. C. Lineberger, J. Chem. Phys. **125**, 133405 (2006).
[11] J. Douady, E. Jacquet, E. Giglio, D. Zanuttini, and B. Gervais, Chem. Phys. Lett. **476**, 163 (2009).
[12] D. M. Neumark, J. Chem. Phys. **125**, 132303 (2006).
[13] W. Müller, J. Flesch, and W. Meyer, J. Chem. Phys. **80**, 3297 (1984).
[14] D. Zanuttini, E. Jacquet, E. Giglio, J. Douady, and B. Gervais, J. Chem. Phys. **131**, 214104 (2009).
[15] J. Douady, E. Jacquet, E. Giglio, D. Zanuttini, and B. Gervais, J. Chem. Phys. **129**, 184303 (2008).
[16] R. A. Aziz and M. J. Slaman, Chem. Phys. **130**, 187 (1989).
[17] F. Y. Naumkin and D. J. Wales, Mol. Phys. **96**, 1295 (1999); D. J. Wales, J. P. K. Doye, A. Dullweber, F. Y. Naumkin, and F. Calvo, http://www-wales.ch.cam.ac.uk/CCD.html for the Cambridge Cluster Database.
[18] J. A. Northby, J. Chem. Phys. **87**, 6166 (1987).
[19] M. Lax, J. Chem. Phys. **20**, 1752 (1952).
[20] E. J. Heller, J. Chem. Phys. **68**, 2066 (1978).